IEEE Access
Multidisciplinary | Rapid Review | Open Access Journal

Received May 19, 2020, accepted May 31, 2020, date of publication June 11, 2020, date of current version June 25, 2020.

Digital Object Identifier 10.1109/ACCESS.2020.3001610

A Low Complexity Design Framework for NFC-RFID Inductive Coupled Antennas

BENOIT COURAUD[1], (Member, IEEE), THIBAUT DELERUYELLE[2,3], REMY VAUCHE[3], DAVID FLYNN[1], (Member, IEEE), AND SPYRIDON NEKTARIOS DASKALAKIS[1], (Member, IEEE)

[1]Smart Systems Group, Heriot-Watt University, Edinburgh EH14 4AS, U.K.
[2]ISEN-Toulon, CNRS, IM2NP, 83000 Toulon, France
[3]Aix Marseille University, Université de Toulon, CNRS, IM2NP, 13397 Marseille, France

Corresponding author: Benoit Couraud (b.couraud@hw.ac.uk)

This research was supported by UKRI via an Engineering and Physical Sciences Research Council (EPSRC) grant with reference EP/L014998/1.

ABSTRACT Inductive Wireless Power and Data Transfer (WPDT) technology has become a vital enabler to the globalisation of Internet of Things. Driven by an increasing demand for data within applications and by the need to reduce the devices footprint by transmitting data and power with the same antenna, power transfer efficiency has become a barrier to WPDT systems' performance. To overcome the limitations of power transfer efficiency, current research focuses on the design of efficient integrated circuitsand does not consider the challenges of inductive antennas' design and system integration. Hence, current system integration methods used in industry to design receivers for WPDT applications still require expensive experimental benchmarking of antennas. This paper introduces a new framework for inductive WPDT systems integration that focuses on the design of inductive coils and tuning capacitances. First, this framework proposes a new planar rectangular coil inductance formula that achieves an average error of 11% based on the testing of one hundred of coils, which out performs the current state of the art. Then, based on a detailed electrical model of both transmitter and receiver of WPDT systems, our design framework computes the coils geometric parameters and tuning capacitances that will optimize the overall efficiency of the WPDT system.Unlike state of the art design approaches, the main advantage of this framework is that it does not require expensive benchmarking of inductive antennas to find the optimal antenna. Verification of our design framework was achieved through a comparative analysis for Very High Bit Rate 13.56 MHz RFID applications. Results indicate an improvement of more than 15% in overall system power transfer efficiency compared to current state of the art methods within a comparatively more cost effective framework. A sensitivity analysis provides an insight and practical guide to implications of manufacturing variances in component parameters.

INDEX TERMS Inductive antennas, near field communication, radio-frequency identification, wireless power and data transmission.

I. INTRODUCTION

Internet of Things (IoT) endpoints in use in 2020 will grow to 5.8 billion, generating $389 billion of revenue around the globe [1]. Each endpoint requires appropriate power supply and data transfer. Ideally, one channel is required for this, as in the case for wireless charging mode for IoT from Near Field Communication (NFC) forum standard. NFC is commonly used in transport, access control, payment, smart devices or identity documents as passports, and consists in wireless communication between a receiver, called Proximity Integrated Circuit Card (PICC) and a reader, called Proximity Coupling Device (PCD). The receiver can be fully or partly supplied by the magnetic field generated by the PCD reader, and hence consists of a coil called inductive antenna that harvests the magnetic field, and a chip supplied by the coil. In the same time as the power transfer occurs, the reader and the receiver communicate by modulating the same magnetic field, that impacts the wireless power transfer capability.

As an example, new generations of electronic passports will store and communicate more information about the passengers, in order to ease control and increase security

The associate editor coordinating the review of this manuscript and approving it for publication was Raghvendra Kumar Chaudhary.

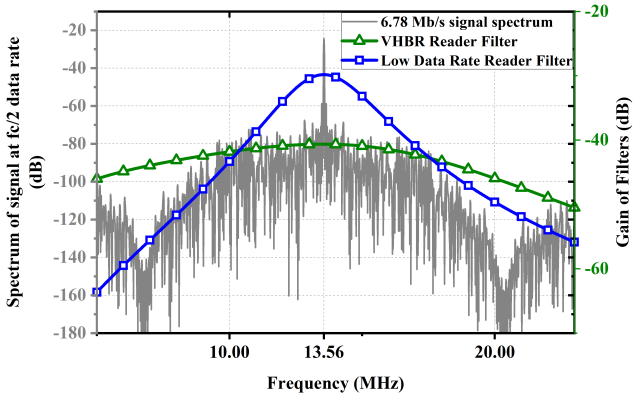

FIGURE 1. Comparison of the gain for a PCD matching circuit for low data rates communications and for VHBR communications.

at the airport borders [2]. Hence, ISO/IEC 14443 standard has evolved towards Very High Bit Rate (VHBR) capability that new generations of passport chips have to comply with, allowing communication speeds up to 6.78 Mb/s with amplitude modulation. This leads to a real challenge for wireless power supply on the same antenna as the one dedicated to data transfer, as PCD readers with high data rate capability have a reduced power transfer efficiency. Fig. 1 shows the spectrum of a VHBR signal at a data rate of 6.78 Mb/s along with the gain of two matching circuits: one designed for low data rates, and one designed for high bit rates as presented in [3]. Most of the signal power is carried at the carrier frequency of 13.56 MHz to allow the reader to power supply the Radio Frequency IDentification (RFID) tag (receiver). The first lobe of data power occupies a bandwidth of 2 times the data rate [4]. Unlike Low-data rate readers VHBR readers have a matching network that filters and isolates the carrier frequency around −80 dB making it difficult to supply the chip. Taking into consideration the above, there is a necessity for optimal designs of the wireless power transfer (WPT) systems. Similarly, different standards also using planar antennas as Qi specifications [5] and NFC Forum [6] require optimal efficient designs. Indeed, NFC forum recently included a Wireless Charging Mode for IoT devices using the same antenna as for the NFC communication, making it necessary to have the best efficiency for fast power transfer at 13.56 MHz, while allowing communication at the usual data rates [7]. To address these challenges, current literature focuses mainly on the design of more efficient chips, by working especially on the rectifier of the chip [8]–[11] or on the data processing part of the chips [12], [13], or on the voltage management at the entry level of the chip [14]. Meanwhile, because of the evolution of standards and because IoT systems are more and more integrated with challenging space constraints, recent literature has also focused on the integration of inductive power transfer capability with planar rectangular or spiral coils into IoT devices [11], [15], [16]. Hence, the consideration of power transfer efficiency between the PCD and the PICC is crucial to achieve good communication, especially in physically constrained environments as smart cards and IoT devices like smart watches or smartphones, where the antenna must be planar, without the possibility to use a magnetic core to increase the efficiency.

Our research proposes a design framework for inductive antennas in Wireless Power and Data Transfer (WPDT) systems. More specifically the work focuses on optimizing the antenna geometry at the receiver and transmitter stages in order to increase the power harvested by the receiver's chip. Today's best practice design methods exploit empirical testing or Radio Frequency (RF) simulations. Compared to them, the proposed design framework is based on a comprehensive system mathematical model that provides an efficient route to an optimal design.

The first contribution of this paper is a formal expression of the efficiency of an Inductive Power Transfer (IPT) system. The efficiency calculation includes the coil parasitic capacitances, resistances and matching networks at the transmitter and receiver levels. All of the aforementioned parameters are typically neglected in state of the art calculations [17], but as we demonstrate through the findings within this paper these parameters are very important for smart cards and NFC applications. Hence, it was necessary to provide a new expression of the efficiency. This paper also proposes a new explicit formula for planar rectangular coils inductance as a function of the geometric parameters. This is of significant value for smart cards, passports but also for IoT applications like smart watches, where spatial constraints prevent engineers from including magnetic cores to boost the efficiency.

The remainder of this paper is structured as follows, section II provides a critical review of current state of the art design methods that are used in the industry to design receivers' antennas. In section III, we present a new framework to design WPDT antennas, which takes into account both the transmitter and the receiver. In section IV, we apply our proposed framework to the design of an RFID passport antenna to demonstrate the advantages compared to state of the art antenna designs.

II. STATE OF THE ART OF ANTENNA DESIGN IN RFID SYSTEMS

To maximize the power transfer efficiency between a transmitter (PCD reader) and a receiver (PICC card), it is necessary to optimize the design of the transmitter and receiver's coils for the particular load or chip of the receiver. The design of a coil consists in determining its geometric characteristics such as the length (a) and width (b) in the case of a rectangular coil, or the outer radius (r_{out}) and the inner radius (r_{in}) in the case of a spiral coil. Geometric characteristics also include the number of turns (N), the gap between each turn (g), and finally the width of the copper segment (w) and its thickness (t), as shown in Fig. 2 and described in [3].

The different methods used in the industry to find the optimal antenna for a given receiver are based on magnetic

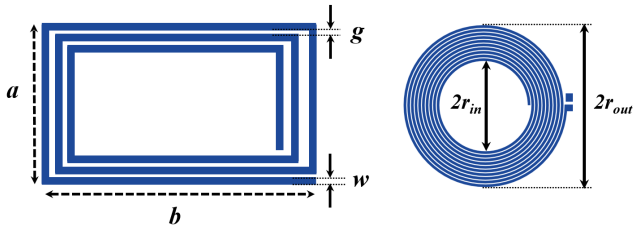

FIGURE 2. Rectangular and spiral planar inductive coil example with N = 3 loops for the rectangular coil.

resonant coupling. Hence, state of the art design methods consider an additional capacitance placed at the output of the receiver antenna, with the aim of determining the antenna geometry and the capacitance value that will achieve a resonant system with the receiver's load at the desired frequency.

However, it is difficult to theoretically determine an accurate coil geometry that achieves resonance for a given load. Also, resonance is not a sufficient condition to maximize the power transfer efficiency, as we will see in section IV-B. Indeed, two coils with the same inductance value but with different number of turns will achieve a different power transfer efficiency. For these reasons, state of the art design methods follow two main phases:

- In the first phase, the optimal geometry of the coil and the value of an additional capacitance are computed in order to theoretically achieve resonance between the coil, the capacitance and the load or PICC chip. This phase is described in II-A.
- In the second phase, described in II-B, an iterative benchmark process is implemented in order to determine the final antenna geometry. In this phase, manufacturers produce many antennas geometries close to the one determined in the first phase, and select the geometry that achieves the best efficiency.

The current section summarizes this approach used in the industry, as it is explained in [18]–[21]. A summary of this procedure is also found in Fig. 3.a.

A. COMPUTATION OF THE OPTIMAL COIL GEOMETRY

Utilising the current state of the art methods, a receiver's coil geometry is computed to achieve a resonant system with the receiver's load and a possible additional capacitance. The following steps are followed to compute this geometry.

1) ELECTRICAL MODEL OF THE RECEIVER

First, the design of an inductive WPDT system starts by determining the electrical model of the receiver and a tuning capacitance value. Indeed, a receiver is composed of a coil antenna, a tuning capacitance, and the load that is constituted by a chip mainly containing a rectifier, a power management system and a wireless communication system. The load impedance Z_L can be modelled as a serial impedance Z_{L_s} (1) or a parallel impedance Z_{L_p} (2), and includes the rectifier and

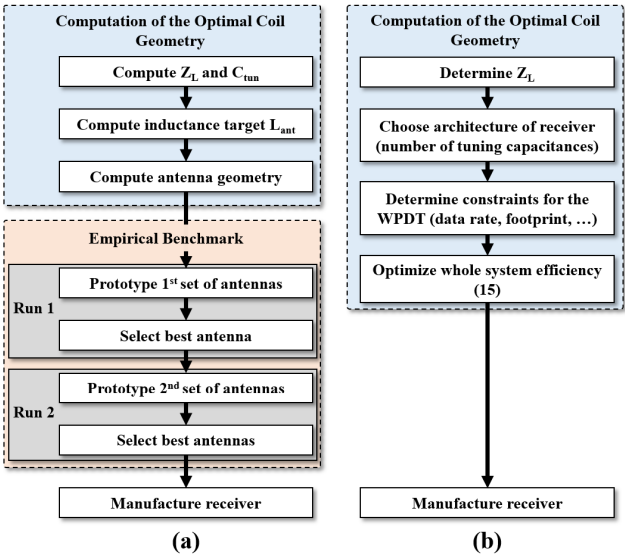

FIGURE 3. Standard antenna design procedure (a) [20] and proposed alternative framework based on efficiency optimization (b).

the electronic components behind.

$$Z_{L_s} = R_s + jX_s \tag{1}$$

$$Z_{L_p} = R_p + jX_p \tag{2}$$

where $R_{s/p}$ and $X_{s/p}$ are the equivalent serial/parallel resistance and reactance of the load respectively. The antenna can be modelled by a simple electric circuit, composed of a resistance and an inductance in serial or by a more complete model with a parasitic capacitance in parallel with the resistance and inductance, as shown in Fig. 4.

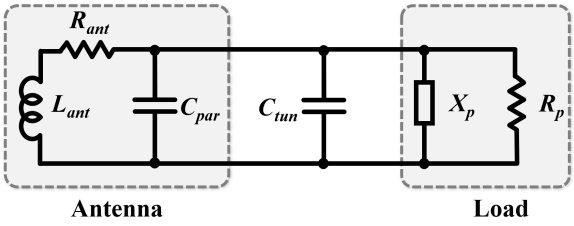

FIGURE 4. Circuit model of a receiver in inductive power transfer systems.

The first step of inductive antennas design is to select an electrical model for the antenna and to determine the value of the complex impedance of the chip Z_L for which the design of the coil will be optimized. This value can be found in data sheets or measured using measurement methods as [22], making sure the measured impedance corresponds to the chip impedance when it is in a working state. The choice for including the parasitic capacitance C_{par} is often due to the angular frequency ω of the application. The higher the frequency, the more important it is to include the parasitic capacitance in the electrical model. However, for simplification purpose, and because state of the art methods rely on trial and errors [18]–[21], the parasitic capacitance

is often neglected in current approaches. As previously mentioned, this step also includes the selection of a tuning capacitance based on the datasheet of the chip.

2) COMPUTATION OF THE COIL INDUCTANCE TARGET VALUE

State of the art methods used in PICC antenna design correspond to magnetic resonant coupling approaches. Hence, they consist in determining the antenna that will resonate with the load's impedance at the desired frequency. The target for the antenna's inductance value is then given as follows:

$$L_{ant} \approx \frac{1}{\omega_0 \left[C\omega_0 - \frac{1}{X_{p_{\omega_0}}} \right]}, \tag{3}$$

where $C = C_{tun} + C_{par}$, with C_{par} the parasite capacitance of the antenna shown in Fig. 4 but usually neglected, C_{tun} the tuning capacitance and $X_{p_{\omega_0}}$ is the equivalent parallel reactance of the load at the targeted angular frequency ω_0. In some applications where several PICCs are physically stacked together, a higher resonance angular frequency than ω_0 is considered in (3). If the load can be modelled as a resistance in parallel with a capacitance C_L, then $X_p = -\frac{1}{C_L\omega}$.

3) COMPUTATION OF ANTENNAS GEOMETRIC PARAMETERS

Once the target value for the inductance has been computed using (3), the geometry of the coil can be determined using simplified formulas that compute the value of the inductance as a function of the coil geometry. Two main categories will be considered in this study: planar *spiral/circular* coils and planar *rectangular* coils, as they are the most widely used in industry. All the geometric parameters of this section are expressed in cm.

a: SPIRAL OR CIRCULAR COILS

Different equations exist in literature to determine planar spiral inductances values from their geometric parameter [18]–[20], [23]–[26]. Only the two most accurate formulas are presented in this study and our decision was based on experimental measurements realized with a Vector Network Analyser at a frequency of 13.56 MHz:

- The authors in [24], [25] proposed a formula repeated in (4), which is based on values from a table to determine the coefficient K_2 as a function of the A/D ratio:

$$L_{ant}(\mu H) \approx K_{2(A/D)} \frac{N^2 D}{2000} \tag{4}$$

  with $D = r_{in} + r_{out}$ and $A = r_{out} - r_{in}$, with $r_{in} = r_{out} - N(w+g)+g$ where w is the copper segment width, N the number of turns, and g the gap between two segments.
- The authors in [23] proposed another simple formula (5) that is a function of 4 coefficients that depend on the antenna geometry (circular, square, octagonal, or hexagonal).

$$L_{ant}(\mu H) \approx \frac{\mu_0 N^2 D c_1}{2} \left[\ln\left(\frac{c_2}{\rho}\right) + c_3\rho + c_4\rho^2 \right] \tag{5}$$

  with $c_1 = 10000$, $c_2 = 2.46$, $c_3 = 0$ and $c_4 = 0.2$ for a circular coil, $\rho = \frac{r_{out} - r_{in}}{r_{out} + r_{in}}$, and μ_0 the vacuum permeability.

b: RECTANGULAR COILS

As for circular coils, rectangular coil antenna value can be approximated by simple equations. Prior research works have proposed formulas, such as *Wheeler* [20], [23], [27] or the one from *NXP* [28], the formula from *Paret* [29], the formula from *Greenhouse*, [19], [30], and finally other approaches that can be found in [18] and [26]. The most accurate formulas based on our measurements are the following:

- The work in [20] and [23] propose a "*Wheeler modified*" formula:

$$L_{ant}(\mu H) \approx k_1 \mu_0 N^2 \frac{A}{1 + \rho.k_2}, \tag{6}$$

  with $k_1 = 23400$ and $k_2 = 2.75$.
- In [30], *Greenhouse* proposed a physics based approach related to *Grover*'s work [26]. However, the complexity of the formulation increases dramatically with the number of turns [19]. The inductance is given by:

$$\begin{aligned} L_{ant}(\mu H) &\approx L_0 + M^+ - M^- \\ &= \sum_i L_{0i} + \sum_{i,j} M_{ij}^+ - \sum_{i,j} M_{ij}^-, \end{aligned} \tag{7}$$

  with $M_{i,j}^+$ and $M_{i,j}^-$ respectively the positive and negative mutual inductance between segment i and j, depending on whether the current flows in the same or opposite direction in these two segments. L_{0i} is the self inductance of segment i of the antenna. Thus, the number of mutual inductances to be computed increases every time the number of turns changes, which makes it hard to implement this approach. The development of each terms of (7) can be found in [30].
- Finally, in [31], *STMicroelectronics* proposes an online tool to compute an inductive antenna inductance based on its geometric characteristics. As for *Greenhouse* approach, this design tool is based on the antenna segments disentanglement method. It is associated with self and mutual inductance calculations using Grover's method based on Geometric Mean Distance and parasitic capacitance calculations. This tool however is proprietary and does not provide an implementable mathematical expression of the inductance in a spreadsheet or solver.

Using (3) and the inductance formulas or tool described above, it is possible to determine the theoretical optimal geometry of the coil to be used for their receiver. However, the previous formulas are not always easy to use or they are not accurate [30], [31] as it will be highlighted in section IV (Fig. 7). Due to this lack of accuracy and because resonance is not sufficient to achieve an optimal efficiency, an iterative empirical process is typically used to determine the final antenna geometry that will achieve an acceptable efficiency

for the whole WPDT system. The following subsection presents an overview of this iterative procedure.

B. EMPIRICAL BENCHMARK

1) PRODUCTION AND BENCHMARK OF A FIRST SET OF ANTENNAS

Once the geometric characteristics of the targeted antenna have been chosen, a statistical design approach is used in order to compensate uncertainties from the formulas listed above. Thus, several antennas are produced with inductance values ranging from 5 to 10% around the targeted antenna. The obtained coil antennas have different lengths, width, and can even have different number of turns.

With the set of coil antennas produced, a benchmark study is realized to select the one that achieves the highest efficiency. To do so, the following steps are run:

- Each antenna is connected to a sample of the receiver chip to create a receiver.
- The obtained receivers are supplied with a chosen transmitter (PCD reader) at different distances, one at a time. When a tuning circuit for resonance is used, each load is tuned with a variable capacitance until the highest voltage is obtained at the input of the chip at the desired frequency.
- The receiver that is supplied and able to communicate at the greatest distance from the transmitter is selected as the optimal one. The corresponding pair of coil antenna and tuning capacitance is selected as the best one.

2) BENCHMARK OF A SECOND SET OF ANTENNAS

Once the optimal antenna from the first set of antennas has been determined, it is often proposed to realize a new set of antennas with geometric characteristics close to the optimal one. A benchmark of this second set is done to determine the optimal antenna from this iteration. An iterative process can be done until the desired efficiency is achieved. At the end, the antenna with which the RFID system achieves the highest efficiency will be used for industrial production, as long as it meets manufacturing requirements.

C. DRAWBACKS OF STATE OF THE ART DESIGN METHODS

The main drawback of these design methods is that it necessitates to produce a large quantity of antennas, and to test all of them individually. This process is time consuming and expensive. This is why this article proposes a new alternative framework for WPDT transmitters and receivers design, that does not require expensive benchmark of coil antennas. Fig. 3.a summarizes the standard design process that was described in this section, and Fig. 3.b displays the new optimization framework that is described in the next section. It shows that the main advantage of the proposed design procedure is to remove the need for benchmarking, which is the most expensive phase of current design methods used in the industry. As it is explained in the next section, this is achieved by introducing a new set of formulas to accurately compute the inductance value as a function of a coil geometry, and by optimizing the efficiency of the power transfer for the whole system instead of only considering the resonance at the receiver level.

III. OPTIMISATION FRAMEWORK FOR ANTENNA DESIGN IN INDUCTIVE WPDT SYSTEMS

In this section, we present a new optimisation framework for the design of coil antennas for inductive WPDT systems, inclusive of tuning capacitances. The approach used for this framework consists in modelling the whole WPDT system in order to determine a formal expression of its efficiency as a function of every design parameter such as coils geometry and tuning capacitances. The optimization framework then consists in maximizing this efficiency by choosing the optimal antennas and capacitances parameters.

As for state of the art methods, the first step is to determine the receiver chip's electric model and its impedance value. As mentioned in section II, this information can be found in the datasheet of the chip, or can be measured directly. In [22], the authors present a method to determine a PICC chip impedance by sending a voltage wave to the chip and analysing the reflected wave, as Vector Network Analysers would do, but with a much higher power. Such high power is necessary to be able to supply the chip, so the measured impedance value corresponds to the working state of the chip.

Once the chip electrical model is known, the proposed framework consists in determining a formal expression of the power transfer efficiency between the transmitter source and the receiver chip. With that formal expression expressed as a function of the design parameters, the goal will be to optimize the design parameters so the efficiency is maximized.

A. THEORETICAL EXPRESSION OF THE EFFICIENCY OF AN INDUCTIVE WPDT SYSTEM

The framework proposed in this paper considers a complete model of the system constituted by the transmitter, the tag and their antennas as displayed in Fig. 5.

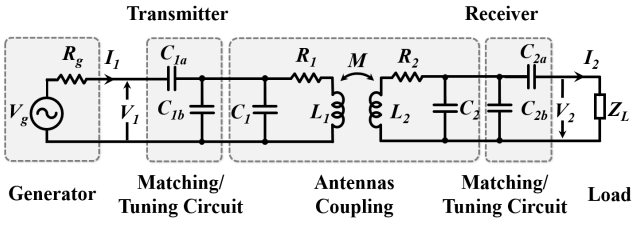

FIGURE 5. Model of an inductive power transfer (IPT) system.

The transmitter is composed of a generator with an internal impedance R_g, a tuning circuit with capacitances C_{1a} and C_{1b}, and an inductive antenna that is modelled by its comprehensive equivalent circuit (R_1, C_1, L_1) with a parasitic capacitance C_1. The receiver is constituted by an antenna with parameters R_2, C_2, L_2, a tuning circuit with parameters

C_{2a}, C_{2b} and the load. The same process can be adapted for symmetric antenna topologies with equivalent components.

Unlike what can be found in the literature, this model includes the resistive losses from the inductances as well as the parasitic capacitance. It also includes the matching networks at both the transmitter and receiver level. These parameters have significant impacts at high frequencies as 13.56 MHz. To formulate mathematically the efficiency of this comprehensive model, it is necessary to transform it into a rearranged model as shown in Fig. 6.

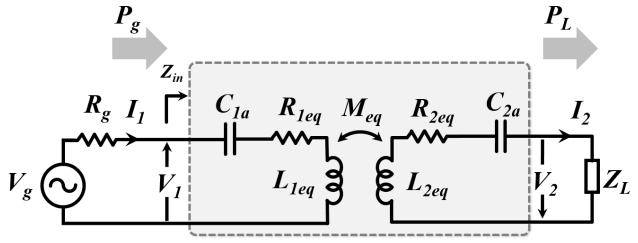

FIGURE 6. Rearranged model of an IPT System, where parasitic capacitances from coils antennas are integrated into the equivalent resistances and inductances.

The manipulation realized between Fig. 5 and Fig. 6 consists in transforming the parallel components into serial components by determining the equivalent parameters. This is what is done by the following formulas that give the equivalent component values for the transmitter.

$$L_{1eq} = \frac{L_1\left(1 - L_1 C_{p_1}\omega^2\right) - R_1^2 C_{p_1}}{\left[1 - L_1 C_{p_1}\omega^2\right]^2 + \left[R_1 C_{p_1}\omega\right]^2}, \tag{8}$$

$$R_{1eq} = \frac{R_1}{\left[1 - L_1 C_{p_1}\omega^2\right]^2 + \left[R_1 C_{p_1}\omega\right]^2} \tag{9}$$

where $C_{p_1} = C_1 + C_{1b}$. (8) and (9) can be simplified if no parallel tuning capacitance is considered and if the antenna is modelled by its simplified circuit by putting $C_{1b} = 0$ or $C_1 = 0$ respectively. But this should not be done for high frequencies applications. As mentioned above, the same transformation is done for the receiver by replacing subscript 1 by 2.

Now that the system has been rearranged and simplified, it is possible to compute its efficiency $\eta = \frac{P_L}{P_g}$ as a function of each parameter, with P_g and P_L the active power provided by the source and received by the receiver's chip respectively. First, as proposed in [17], [32] we consider a two ports model, highlighted by the grey area in Fig. 6, with the mutual inductance M_{eq} between the transmitter and receiver coils. The voltages V_1 and V_2 can be expressed as follows:

$$\begin{bmatrix} V_1 \\ V_2 \end{bmatrix} = \begin{bmatrix} Z_{11} & Z_{12} \\ Z_{21} & Z_{22} \end{bmatrix} \begin{bmatrix} I_1 \\ I_2 \end{bmatrix} = \begin{bmatrix} R_{1_{eq}} + j\omega L_{1_{eq}} & -j\omega M_{eq} \\ -j\omega M_{eq} & R_{2_{eq}} + j\omega L_{2_{eq}} \end{bmatrix} \begin{bmatrix} I_1 \\ I_2 \end{bmatrix} \tag{10}$$

where ω is the angular frequency of the current I_1, and V_1, V_2, I_1 and I_2 are defined in Fig. 6. V_2 can also be expressed as $V_2 = [R_s + jX_s]I_2$, with the chip impedance Z_L modelled as a serial impedance $Z_L = R_s + jX_s$ that includes the rectifier and the electronic components behind. Thus, expressing I_2 as a function of V_1 from (10), the active power accepted by the receiver chip is given below:

$$P_L = R_s |I_2|^2 = \frac{k^2 L_{2_{eq}} R_s}{L_{1_{eq}}} \frac{|V_1|^2}{\left[\omega L_{2_{eq}}\left(1 - k^2\right) + X_s\right]^2 + R_s^2}, \tag{11}$$

where $k \in [0, 1]$ is the coupling coefficient $k = \frac{M_{eq}}{\sqrt{L_{1_{eq}} L_{2_{eq}}}}$ between the transmitter and receiver antennas that can be approximated by the expression [33]:

$$k(d) \approx \frac{r_t^2 r_r^2}{\sqrt{r_t r_r}\left(d^2 + \max(r_t, r_r)^2\right)^3}, \tag{12}$$

with r_t and r_r the average external radius of the coil of the transmitter and the receiver respectively, and d the distance between the two coils. If (12) is more suitable for large distances d compared to the radii r_t and r_r, it still provides accurate results at small distances [34].

Then, the active power generated by the source P_g is given as shown below:

$$P_g = |V_g|^2 \Re\left\{\frac{1}{R_g + Z_{in}}\right\}, \tag{13}$$

with Z_{in} determined by:

$$\begin{aligned} Z_{in} &= Z_{11} - \frac{Z_{12} Z_{21}}{Z_{22} + Z_L} \\ &= \left[R_{1_{eq}} + jL_{1_{eq}}\omega\right] + \frac{\left(\omega M_{eq}\right)^2}{\left[R_{2_{eq}} + jL_{2_{eq}}\omega\right] + Z_L}. \end{aligned} \tag{14}$$

This yields to the following expression of the efficiency η for a distance d between the transmitter (PCD) and the receiver chip of impedance Z_L:

$$\eta(d) = \frac{\Re\{Z_L\}\left(\omega M_{eq}(d)\right)^2}{R_g + R_{eq}^2\left[R_{1eq} + \frac{\left(\omega M_{eq}(d)\right)^2}{R_{eq}}\right] + X_{eq}^2 R_{1eq}} \tag{15}$$

with $X_{eq} = \mathrm{Im}\{Z_L\} + L_{2eq}\omega - \frac{1}{C_{2a}\omega}$, $R_{eq} = R_{2eq} + \Re\{Z_L\}$, $M_{eq}(d) = k(d)\sqrt{L_{1eq} L_{2eq}}$.

Thus, (15) provides an expression of the overall system efficiency as a function of the transmitter (PCD) and receiver (PICC) coils inductance and tuning capacitance C_{2b}. Although (15) looks similar to Inductive power Transfer (IPT) systems efficiency approximations found in the literature [17], [32], it is actually different, as the expression also includes (8), (9) and all the parameters mentioned above X_{eq}, R_{eq}, M_{eq}. Indeed, unlike the simplified versions of IPT systems efficiency, (15) considers the matching losses, as well as the impacts of parasitic capacitance and resistance for the coils, which can be significant for IPT at 13.56 MHz. This is the first main contribution of this work.

Then, in order to find the optimal coils geometry, it is required to express the inductances L_1 and L_2 as functions

of the coil antennas geometry and include them in the design parameters. As it was mentioned in section II, existing formulas are either not accurate enough or not implementable into a solver, as for [31]. Thus, the next subsection proposes an accurate formula that can be implemented in (15) in order to express the efficiency as a function of every design parameter. This will be the second main contribution of this study.

B. COMPUTATION OF PLANAR COILS INDUCTANCE

It was discussed in Section II that accurate formulas exist in literature for spiral/circular coils for frequencies under the hundreds of MHz range ((4) and (5)). Hence, in the case of spiral planar antennas, we propose to use an average of these formulas to obtain a good estimation of L_1 and L_2 as functions of the outer coils radius r_{out}, the number of turns N, the width of the copper segment w and g the gap between two segments. To simplify the implementation in a solver, we also propose to reformulate (4) as follows:

$$L_{ant}(\mu H) \approx 12.17\left[1 - \ln\left(\frac{A}{D}\right)\right]\frac{N^2 D}{2000}, \tag{16}$$

with $D = r_{in} + r_{out}$ and $A = r_{out} - r_{in}$, with $r_{in} = r_{out} - N(w + g) + g$ all in cm.

For rectangular coils, it was quickly mentioned that existing formulas are either not easily implementable into a solver or have a lack of accuracy, which can have considerable impacts on the optimization of (15). We tested state of the art formulas over one hundred antennas geometries (as shown in section IV) and concluded that *STMicroelectronics* method [31] and *Greenhouse*'s [30] are the most accurate methods. However, [31] is not compatible with the optimization of (15) as no formula is available and [30] requires significant implementation efforts as the number of equations is proportional to the number of turns.

Hence, a new formula is proposed in Appendix to estimate the inductance value of a planar rectangular coil. The proposed formula consists in a simplification of *Greenhouse*'s method [30] so it can easily be used in a numerical optimization. The adopted model for a rectangular coil is the one presented in Fig. 4 with a parasitic capacitance in parallel with a resistor and an ideal inductance, which is a necessary choice for high frequency applications. Indeed, the power that is transferred by the coil to the receiver's load is equal to the power that is harvested by the coil, subtracted by the ohmic losses in the windings, but also subtracted by the reflected power at the load's end.

Ohmic losses inside the windings correspond to the active power losses due to the DC and AC resistance of the coil, that increases with the frequency. Therefore, it is important to consider the resistance of the coil in our model as it impacts the overall efficiency. Secondly, the reflected power at the receiver load's end is due to an impedance mismatch between the coil and the load. Therefore, it is also required to consider the impact of the resistance and the stray capacitance in our model in order to determine accurately the complex impedance of the coil. Indeed, the parasitic capacitance tends to lower the reactance of the coil when the frequency increases. Hence, if the resistance and stray capacitance were not included into the model, the efficiency of the power transfer given by (15) would not capture all the losses at high frequencies and the optimization of (15) would not lead to an optimal design. It can be simplified into a serial model constituted by an equivalent inductance $L_{1/2eq}$ in serial with an equivalent resistance $R_{1/2eq}$, as shown in Fig. 6 by using (8) and (9) with $C_{p_1} = C_1$ or $C_{p_2} = C_2$, the parasitic capacitances. The following development computes the inductance $L = L_1$ or L_2 and the stray capacitance $C_{par} = C_1$ or C_2 that can then be substituted into (8) and (9). If the considered application requires an extra parallel capacitance C_{1b} or C_{2b} for resonance or tuning, it can be added in C_{p_1} or C_{p_2} as proposed by (8). Following [30], the inductance L (L_1 or L_2) is given by (17).

$$L(nH) = L_0 + M_+ - M_-, \tag{17}$$

with L_0 the sum of the self-inductances of all the straight segments and $M_+/-$ are the sum of the positive/negative mutual inductances between two segments where the current flows in the same/opposite direction respectively. These three terms must be expressed as functions of the coil length b, the coil width a, the segments width w, the segments thickness t, the gap between two segments g (Fig. 2) and finally the number of turns N. The Appendix section describes the computation of L_0, M_+ and M_-.

For the parasitic capacitance computation, several approaches exist in the literature to determine analytically the parasitic capacitance of an inductance [35]–[45]. The parasitic capacitance corresponds to the sum of all the parasitic capacitances between the turns of the coil, but also between the copper segments and the environment of the coil, as the ground or the casing. Most of the previous works on parasitic capacitance follow a physics based approach. Among these works, only [43]–[45] consider planar inductances. However, [43] applies only to coils with very thick copper wires (t), for which the parasitic capacitance decreases with the number of turns, which is the opposite to what is observed in the case of thin copper segments used in NFC. Also, the approach in [45] depends on a capacitance per unit length between adjacent metal turns that is not explicitly determined. Finally, the work in [44] is the closest to our requirements, although it only considers spiral coils, and proposes a formula that depends on the effective height of the electrical flux between two adjacent turns, which is difficult to determine. As [44] only applies to circular spiral antennas, it did not demonstrate good enough results based on the hundred rectangular coils geometries that were tested (with an average error of 75%). Hence, we propose an empirical formula (18) based on one hundred rectangular coils tested by the authors with number of turns between 2 and 6, as it is what is mostly used for rectangular planar coils [33]. The parasitic capacitance is directly computed from the number of turns N, the width of

the copper w, and the size of the coil a, b, all expressed in cm in (18).

$$C_{par} = \frac{\epsilon_0\sqrt{(N-1)}}{400}\sqrt{ab}\left[\ln\left(\frac{w}{g}\right)+16\right] \quad (18)$$

where ϵ_0 is the vacuum permittivity. This proposed formula gives similar trends and order of magnitude as [44] for planar inductances' parasitic capacitance, with an average error below 10%.

Finally, the serial resistance of the coils must also be accurately estimated as it has two main impacts on the overall efficiency: first, the resistance of the coil is used in the matching with the receiver's load. Second, the resistance of the coil is the source of ohmic losses in the system. Hence, an inaccurate estimate of the resistance will not allow the designers to determine the coil geometry that maximizes the power transfer efficiency. A coil's resistance consists in a DC resistance and an AC resistance, consequence of the skin effect when the frequency increases (unequal distribution of the current density in the segments due to the magnetic field distribution inside the wire) [46]–[50]. A comprehensive approach for the serial resistance computation can be found in [51], although the following simplified formula from [19] gives accurate enough results at frequencies in the MHz range:

$$\begin{aligned} R_{1\text{ or }2} &= R_{DC} + R_{AC} \\ &= \frac{\sum b_k + \sum a_k}{100}\left[\frac{1}{S\sigma} + \frac{1}{\sigma\delta_p(w+t)}\right] \end{aligned} \quad (19)$$

with $\sum b_k$ and $\sum a_k$ defined in the Appendix section (in cm) (28), (29). $S = w \cdot t$ is the section of a conductor segment, σ is the conductor's material conductivity (in S/m), and $\delta_p = \frac{1}{\sqrt{\pi\mu\sigma f_0}}$ is the skin depth (in m). $\mu = \mu_0\mu_r$ is the permeability of the conductor material (in H/m), and f_0 is the AC signal frequency.

The obtained equivalent inductance $L_{\text{i eq}_{i\in\{1,2\}}}$ is computed from (8) by replacing L_1 by L (17) and C_{p_1} by C_{par} (18).

C. OPTIMIZATION OF THE EFFICIENCY OF A WPDT SYSTEM

Using the proposed inductance computation formula, it is now possible to find the geometries of the coils G and the tuning/matching circuits capacitances C_{1a}, C_{1b}, C_{2a}, C_{2b} that will optimize (15), as shown in the optimization problem described in (III-C). The design becomes now an optimization problem, where the objective is to maximize (15) by changing the geometry parameters and tuning capacitances, while meeting the constraints such that all distances must be positive and fit into normalized packaging. Additionally, the inductances and geometry parameters are linked together by (8), (9), (12), (17) - (34). Due to the number of turns having to be an integer, the obtained optimization problem is a Mixed Integer Non Linear Problem (MINLP) that can be implemented in any spreadsheet or optimization software (MATLAB, R or GAMS), and optimized using an appropriate non linear solver. The expression of this problem is given below:

$$\begin{aligned} \underset{G,\, C_{1a},\, C_{1b},\, C_{2a},\, C_{2b}}{\text{maximize}} \quad & \eta \quad (15) \\ \text{subject to} \quad & \text{distances} \geq 0 \\ & N \in \mathbb{N} \\ & (8),\ (9),\ (12), \\ & (17) - (34). \end{aligned}$$

The solution of this problem corresponds to the optimal geometry and capacitance values that maximize the efficiency of the WPDT system.

Other constraints can be added as for example a lower limit for the efficiency within a certain range of frequencies in order to ensure the communication capability of the receiver and transmitter at a given data rate.

This problem was optimized using population-based evolutionary algorithm available in Excel. Although evolutionary algorithms take greater computing time to converge, they are best fitted to find global extrema in such constrained non-convex optimization problems [52]. Based on the extensive testing that was done on a computer with an i5 processor at 1.7GHz, the CPU processing time for solving the optimization problem was below 20 seconds for all tested geometries.

The next section presents the results obtained with this framework for the design of VHBR Smart Cards.

IV. EXPERIMENTAL RESULTS

This section presents a validation of the proposed inductance formula for rectangular planar inductive coils by comparing its accuracy with other state of the art approaches. Then, (15) is validated based on experimental measurements, and the proposed optimization is used to find the optimal antennas for two RFID VHBR chips.

A. VALIDATION OF PLANAR RECTANGULAR COIL INDUCTANCE FORMULA

In order to compare the proposed formula with existing state of the art formulas, we have generated 100 random geometries for rectangular coil antennas. They have random number of turns between 2 and 6, random sizes a, b, *width* and *gap*, and we compared the value given by all aforementioned formulas and a reference.

The reference consists in real measures for half of the coil antennas, and HFSS software simulated inductances for the other half. Fig. 7 shows the comparison of all the inductance values for the 50 highest turn numbers coils antennas. Values differ considerably for some formulas and antennas. According to the benchmark realized on these 100 antennas, the approaches proposed by *STMicroelectronics* in [31], by *Greenhouse*, and the proposed new formula are the most accurate. Table 1 summarizes the results of this comparison for rectangular planar coil antennas. As a reminder, while *Greenhouse*'s approach is one of the most accurate, it is

TABLE 1. Comparison of the accuracy of different inductance computation methods.

Method	Average error (%)	Ease of use
Paret [29]	91	++
Wheeler Modified [23]	50	++
Greenhouse [30]	11	-
NXP [28]	48	+
STMicroelectronics [31]	13	- -
Proposed Formula	11	+

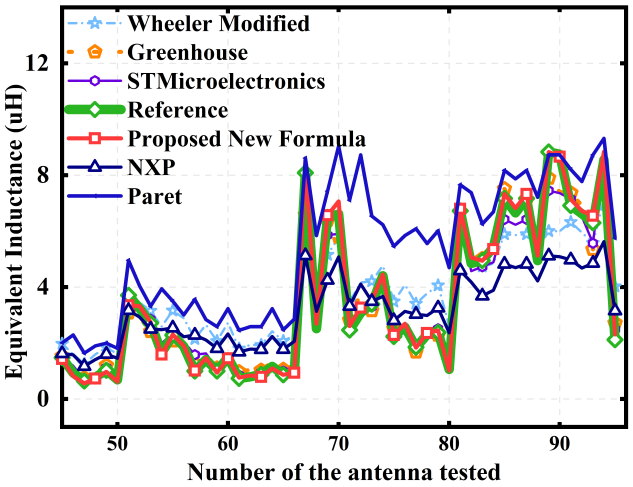

FIGURE 7. Graphical comparison of different inductance calculation methods [23], [28]–[31] for 100 planar rectangular antennas.

also one of the less practical to implement, as the number of equations to implement to compute the inductance is proportional to N. Similarly, *ST*'s approach cannot be used as it does not provide any explicit formula implementable in a solver to optimize (15). Hence, Table 1 shows that the proposed formula is the best formula in terms of accuracy while being quite easily implementable in a solver, even if this requires to implement all equations mentioned in Appendix, independently of the number of turns.

B. VALIDATION OF THE PROPOSED DESIGN FRAMEWORK

To validate the overall design framework, the best way is to demonstrate that the proposed optimization function, i.e. the system power transfer efficiency η given in (15), is an accurate function of the coils' geometry and capacitances even for high frequency applications as 13.56 MHz. Indeed, the validation of the accuracy of (15) through a comparative analysis with experiments implies that the analytical optimization of (15) will lead to the real optimal design. To demonstrate the accuracy of (15), we propose to compare the theoretical efficiency given by (15) with measured efficiencies over 20 coils that were manufactured to supply two different industrial NFC chips. These chips are Very High Bit Rate compatible, which makes their power supply a real challenge at their highest data rate. The several coil geometries were rectangular coils geometries generated randomly around the optimal value found after optimizing (15).

To realize this experimentation, [22] was used to determine the complex impedances of the two chips. For each chip, the optimal design was computed by solving the optimization problem mentioned in section III and implemented The antennas were printed and connected to their corresponding chip. Other coil antennas were generated by randomly changing geometric parameters by $+/-10\%$ compared to the optimal designs for each chip. This way, ten antennas were obtained for each chip in order to constitute ten receivers for each chip. Accordingly, twenty receivers were produced to realize the tests, and each of them was composed of one antenna, one sample of the two chips, and a tuning capacitance C_{2b} or none for some receivers. To determine the experimental efficiency of the WPDT systems, a controllable RFID reader with a known antenna was used to communicate with each of the receivers, using the ISO 10373 test platform from [53], as shown in Fig. 8 and 9. The power of the RFID reader was increased until each receiver was able to respond, in which case the power received by the load (chip) was equal to the wake up power of the chip. Thus, the power harvested by the chip was the same for every receiver using the same chip. The *experimental efficiency* of the RFID system is then proportional to the inverse of the required RFID reader power to wake up the chip and will be compared to the *theoretic efficiency* of the system, which was computed using (15).

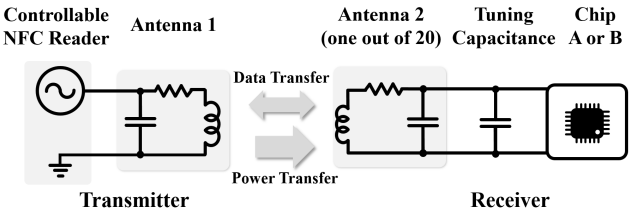

FIGURE 8. Setup for testing of the efficiency of one of the 20 NFC IPT systems tested.

The results were then normalized for each chip as the two chips have a different wake up power that is not known accurately. The comparison of the theoretical and experimental efficiencies are presented in Fig. 10.

The theoretical optimal designs for each chip, implemented in receivers 1 (for chip A) and 11 (for chip B) correspond to the maximum efficiencies measured over all 20 receivers, which validates the proposed design framework. Other receivers determined by small variations in geometric and capacitance parameters obtained lower theoretical efficiencies that are well correlated with measured efficiencies. Indeed, the computed theoretical efficiencies given by (15) match the experimental measured efficiencies with an average error below 10%. If the theoretical and experimental efficiencies do not match perfectly for some receivers (maximum error of 22%), they evolve the same way

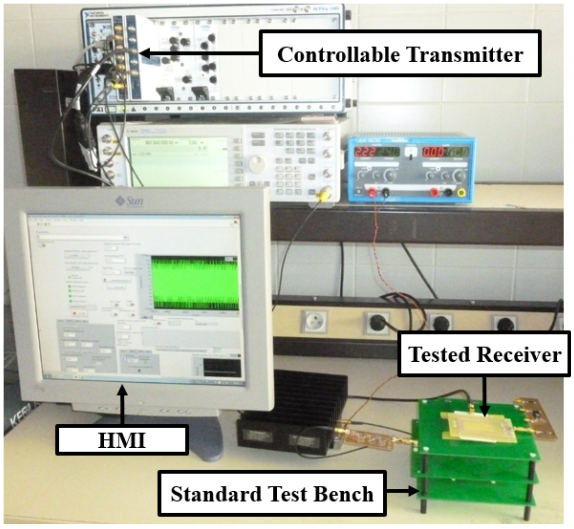

FIGURE 9. Experimental test bench for measurement of power and efficiency of an NFC IPT system.

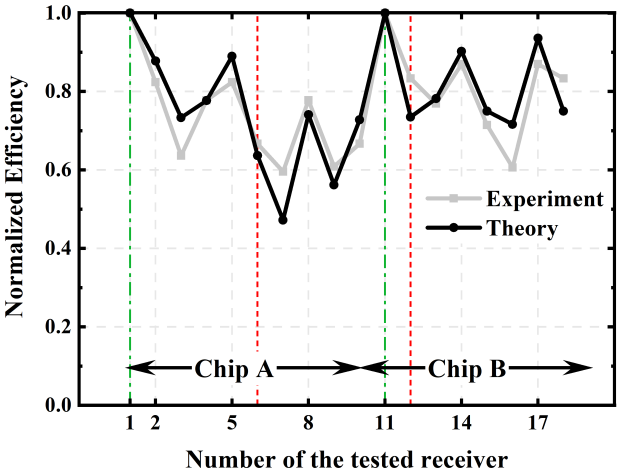

FIGURE 10. Comparison of the experimental normalized efficiency with the normalized theoretical efficiency from (15) for the two chips. The optimal receivers' design is highlighted with green dashed lines (receivers 1 and 11), and receivers obtained from state of the art methods are highlighted with red dotted lines (receivers 6 and 12).

among the different receivers, which shows that using (15), we can accurately rank the performance of each receiver, which is the aim of the approach. The high values of error are mainly explained by the inaccuracy in the load impedance's measurements that has large or small impacts on the system efficiency depending on the coil antenna's inductance value. Moreover, it is worth noting that for both chips, the optimal design was obtained for non-resonant coupling, as the optimized tuning capacitance's value C_{2b} was 20% lower than the one that would have achieved the resonance in the receiver. Indeed, the advantage of adopting a whole system approach is that the whole system's efficiency is considered, including the magnetic field harvesting part. State of the art methods neglect this aspect and focus only on the resonance of the receiver. This experimentation shows that the optimal design might be obtained by favouring the energy harvested by the coil and the reduction of the reflection within the receiver compared to the search for a resonant system.

Hence, WPDT systems' efficiency given in (15) can be considered as accurately representative of the real efficiency. Optimizing it by determining the optimal antennas geometric parameters will result in an optimal RFID system design at a much lower cost than state of the art methodologies that require several trials to obtain a close to optimal design. Finally, the antenna design from state of the art methods presented in section II and implemented in receivers 6 and 12 (highlighted by red dotted line in Fig. 10, with only one set of antenna benchmarked) showed a much lower efficiency (more than 15% below) than the optimal designs found by optimizing (15).

The proposed framework allows WPDT systems designers to achieve close to optimal designs without the need for expensive testing through coil benchmarking. However, it relies on the capability of manufacturing processes to meet the requirements for these optimal geometric dimensions. Thus, in the next section, we propose a sensitivity analysis and discuss what are the impacts of a small variation of the design parameters values on the overall efficiency.

C. SENSITIVITY ANALYSIS

In this section, we explore the sensitivity of the efficiency to manufacturing processes or changes in design. First, we study the impacts of geometric parameters on the inductance value of planar coils. Then, we determine the design parameters that impact most the efficiency in wireless power transfer systems.

1) IMPACT OF DESIGN PARAMETERS ON RECTANGULAR COILS' INDUCTANCE

To study the sensitivity of an inductance value to manufacturing process, we have generated several random geometries. For each of these geometries, we have changed one parameter at a time and computed the inductance value of the new geometry. The parameters that were changed are the gap g, the width of the copper segment w, and the lengths a and b or external diameter for spiral coils. Fig. 11 displays the average sensitivity of the inductance to the design parameters. It shows that a coil inductance, rectangular or spiral, is much more sensitive to the copper width and the gap than to the length or radius of the coil. Indeed, Fig. 11 shows that the value of a coil inductance can be 20% smaller when the copper width is increased by 0.32 mm. Hence, manufacturing processes must ensure accurate dimensions for the gap and copper width of the coils, with tolerance error below 0.1mm to ensure 90% of the theoretical efficiency.

2) SENSITIVITY OF INDUCTIVE WPDT SYSTEMS' EFFICIENCY

It is also interesting to study the impact that each design parameter has on the overall system's efficiency. To realize this study, each design parameter (transmitter and receiver's coil antennas geometries and tuning capacitances) has

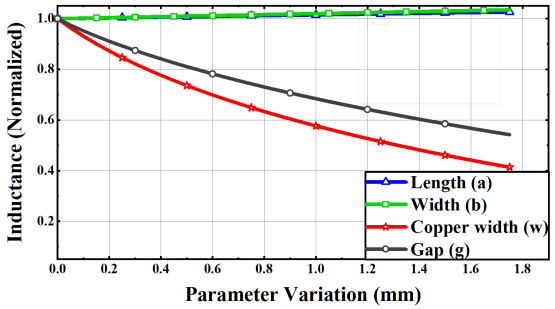

FIGURE 11. Impact of design parameters on a coil inductance value. The parameter variation corresponds to a positive increase of the considered parameter compared to its nominal value. The resulting inductance values are normalized to the inductance corresponding to the nominal parameters.

been modelled as a random variable following a normal distribution with a standard deviation expressed as shown in Table 2.

TABLE 2. Tested standard deviations for design parameters.

Parameter	Standard Deviation
Number of turns	0.8
Lengths / Radius (a, b, r_{out})	5 mm
Thickness / Gap (w, g)	0.15 mm
Capacitances	1.5 pF

Statistical design was used to generate 50 random systems (antennas geometries and capacitances). For each of these systems, the efficiency η was computed in order to assess the impact of each random variable on the power transfer efficiency. This impact was captured by recording the resulting efficiency's standard deviation in each case, as shown in Fig. 12.

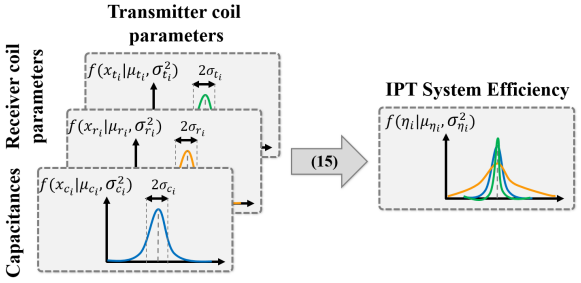

FIGURE 12. Statistic design methodology for sensitivity analysis.

Table 3 displays the impacts of the design parameters on the power transfer efficiency. It shows that the variability of the transmitter's coil antenna parameters are less significant in comparison to the receiver coils antenna parameters. We can also highlight the impact that manufacturing processes can have on the overall system efficiency by focusing on the receiver's coil design parameters. Similar to what was done in subsection IV-C1, we have computed the impact of

TABLE 3. Sensitivity of efficiency to design parameters' variation.

Parameter	Efficiency's Standard Deviation
Transmitter Coil's Geometry	2.5 %
Receiver Coil's Geometry	10 %
Tuning Capacitances	4.6 %

the receiver's coil design parameters on the overall system efficiency. Fig. 13 shows the efficiency evolution when geometric parameters of the receiver's coil are increased by steps of 0.05 mm. As for the coil's inductance value, the gap (g) and the copper width (w) have the greatest impact on the overall efficiency, and must receive particular attention in the manufacturing process.

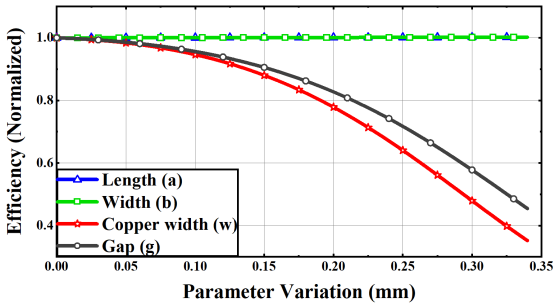

FIGURE 13. Impact of the receiver's coil geometric parameters on the overall system efficiency.

It can be concluded from this sensitivity study that when designing an IPT system, the design and manufacturing of the receiver's antenna must receive particular attention in order to reach the expected overall efficiency. Indeed, a small deviation in the antenna geometric parameters, as the gap and the copper width, can have a significant impact on the system's efficiency.

V. CONCLUSION

To increase the efficiency of inductive Wireless Power and Data Transfer systems, the current practice is to increase the efficiency of Integrated Circuits of transmitters and receivers. However, it was shown that the antenna and matching network design also have a significant impact on the overall system's efficiency. Hence, this work focussed on the design of planar inductive antennas and tuning capacitances, which are extremely relevant for WPDT systems with integration space constraints, as smart cards, passports and NFC applications, where it is not possible to include a magnetic core to boost the efficiency.

This study proposed a new design framework based on a comprehensive system approach. This framework aims to determine the optimal coils geometry and capacitances values in WPDT systems operating at high frequencies in the MHz range. The efficiency of a complete IPT system was formulated as a function of all the design parameters, and especially the coils' geometric parameters, in order

to allow a theoretically optimal design. This efficiency formulation is new in the sense that it now includes the matching consideration at the transmitter and receiver level as well as the parasitic capacitance and resistance from the inductances, which are necessary to include for high frequencies applications such as NFC applications. To achieve such a formulation, we first developed a new expression for the inductance of planar coils as a function of their geometry. Based on an exhaustive benchmark of one hundred different coils, the new inductance formula showed an accuracy of 89%, which is the highest accuracy as compared with other existing inductance computation methods. Using these new formulations, several VHBR RFID receivers were manufactured in order to compare the computed theoretical efficiency with experimental measurements. The efficiency formula showed an average accuracy of 10%, which validates the proposed expression. Finally, we optimized this formula for two VHBR chips in order to determine the optimal antenna geometry and capacitance. The resulting receivers achieved an average increase in efficiency of more than 15% compared to state of the art antennas design method, which validates the proposed framework for WPDT system design. It also achieved such results at a lower cost, as no empirical design was needed to achieve these results, which makes it a very competitive design method for industrials in the RFID sector. It was also shown that the power transfer efficiency is not very sensible to the transmitter's antenna geometry as compared to the receiver's. Hence, this ensures that optimal designs for receivers obtained by the proposed framework will have a good interoperability with existing readers. This design framework can also be used for other applications were planar coils are used, as some Qi compliant IoT devices.

APPENDIX
RECTANGULAR COILS INDUCTANCE CALCULATION

This Appendix provides a new method for the computation of the inductance of a rectangular planar coil based on its geometric parameters defined in Fig. 2, that shows a rectangular planar inductive coil with 3 turns, to which all the formulas correspond. The inductance is given by (17), and this section explains the computation of L_0, M_+ and M_-. First, L_0 can be expressed as follows, where (20) is a generalization of the formula proposed in [30]:

$$L_0(nH) = 4N.2l_{avg}\left[\ln\left(\frac{2l_{avg}}{w+t}\right) + 0.50049 + \left(\frac{w+t}{3l_{avg}}\right)\right] \tag{20}$$

where L_0 is in nH $l_{avg} = \frac{a_{min}+b_{min}}{2}$ is an average length for all segments, with a_{min} the minimal width and b_{min} the minimum length in the coil defined as follows:

$$\begin{cases} a_{min} = a - 2\left(N.w + [N-1]\,g\right), \\ b_{min} = b - 2\left(N.w + [N-1]\,g\right). \end{cases} \tag{21}$$

Then, M_+ can be computed as in [30]:

$$M_+ = 2\left[M_+^l + M_+^w\right] \tag{22}$$

where M_+^l is the positive mutual inductance for segments in the length orientation, and M_+^w the positive mutual inductance for segments in the width orientation given as follows:

$$M_+^l = 2\sum_{i,j=0,i<j}^{N-1} M_{4i+1,4j+1} \approx N\,(N-1)\,M_{+_{avg}}^l \tag{23}$$

with $M_{+_{avg}}^l = 2\,b_{avg}Q_{+_{avg}}^l$ as in [30] with the introduction of averaged terms b_{avg} and $Q_{+_{avg}}^l$, in order to compute quickly the average positive mutual inductance, that are given by:

$$Q_{+_{avg}}^l = \ln\left[\left(\frac{l_b}{d_+}\right)_{avg} + \sqrt{1+\left(\frac{l_b}{d_+}\right)_{avg}^2}\right] - \sqrt{1+\left(\frac{l_b}{d_+}\right)_{avg}^2} + {}^1\!/\!\left(\frac{l_b}{d_+}\right)_{avg} \tag{24}$$

where d_+ corresponds to the distance between two segments considered for the mutual positive inductance, and lb represents the smaller length of the two segments considered for positive mutual inductance. Compared to the original Greenhouse method where the mutual inductance parameter Q_+ is computed as the sum of the positive mutual inductances of all segments combinations, it has been chosen here to compute an average parameter $Q_{+_{avg}}^l$.

The term $\left(\frac{l_b}{d_+}\right)_{avg}$ from (24) is an average of the ratios between the lengths of the considered segments and their distance between each other. According to [30], if the coil is constituted of only one turn, the positive mutual inductance will be 0. If there are two turns, there will be one term for the computation of the mutual positive inductance, which will be equal to $\frac{b-(w+g)}{w+g}$. If there are three turns, there will be three terms for the calculation of $Q_{+_{avg}}^l$, which will correspond to the three following $\frac{l_b}{d_+}$ ratios: $\frac{b-(w+g)}{w+g}$, $\frac{b-2(w+g)}{2(w+g)}$, $\frac{b-3(w+g)}{w+g}$. Thus, the average term $\left(\frac{l_b}{d_+}\right)_{avg}$ can be computed as follows:

$$\left(\frac{l_b}{d_+}\right)_{avg} = \frac{b-(N-1)(w+g)}{\delta_+(w+g)} \tag{25}$$

where $\delta_+(w+g)$ represents the harmonic mean of the denominators of all the $\left(\frac{l_b}{d_+}\right)$ ratios mentioned above ($w+g$, $2(w+g)$, $w+g$ in the example mentioned above), with δ_+ computed as follows:

$$\begin{aligned}\delta_+ &= \frac{\sum_{k=1}^{N-1}(N-k)}{\sum_{k=1}^{N-1}\frac{N-k}{k}} \\ &\approx \frac{1}{2}\frac{N(N-1)}{N\left[\ln(N-1)+0.57721+\frac{1}{2(N-1)}\right]-(N-1)}\end{aligned} \tag{26}$$

where the approximation of denominator's harmonic series has been used with 0.57721 being an approximated value of the *Euler - Mascheroni* constant.

Then, b_{avg} also needs to be explicated in order to compute (23), and is given below:

$$b_{avg} = \frac{\sum_k b_k}{2N} \tag{27}$$

where $\sum_k b_k$ corresponds to the sum of the length of all segments in the length orientation. It can be computed by the following equation, corresponding to the geometry shown in Fig. 2:

$$\begin{aligned}\sum_k b_k &= b{-}w + \sum_{k=0}^{2(N-1)} b - w - k(w+g) \\ &= (2N-1)\left[b{-}w - (w{+}g)(N-1)\right]{+}b{-}w. \end{aligned} \tag{28}$$

For M_+^w, the same development can be done, replacing $Q^l_{+_{avg}}$ by $Q^w_{+_{avg}}$ (a function of $\left(\frac{l_a}{d_+}\right)_{avg}$ obtained by changing b by a in (25)) and b_{avg} by $a_{avg} = \frac{\sum_k a_k}{2N}$, the equivalent of b_{avg} for the width, with $\sum_k a_k$ given by the following formulation (still based on Fig. 7):

$$\begin{aligned}\sum_k a_k &= a{-}w + \sum_{k=0}^{2N-1} a - w - k(w+g) \\ &= N\left[2(a-w) - (w+g)(2N-1)\right]. \end{aligned} \tag{29}$$

Finally, the term M_- from (17) has to be computed the same way, with some minor differences due to geometry considerations based on Fig. 7. Indeed, M_- is given by the following equation:

$$M_- = 2\left[M_-^l + M_-^w\right] \tag{30}$$

with M_-^l given by:

$$M_-^l = 2\sum_{i,j=0, i<j}^{N-1} M_{4i+1,4j+3} \approx N^2\left[2b_{avg}Q^l_{-_{avg}}\right] \tag{31}$$

where the average term $Q^l_{-_{avg}}$ is defined as for the positive mutual inductance:

$$\begin{aligned}Q^l_{-_{avg}} = \ln\Bigg[&\left(\frac{l_b}{d_-}\right)_{avg} + \sqrt{1+\left(\frac{l_b}{d_-}\right)^2_{avg}}\Bigg] \\ &- \sqrt{1+\left(\frac{l_b}{d_-}\right)^2_{avg}} + {}^1\Big/\left(\frac{l_b}{d_-}\right)_{avg}\end{aligned} \tag{32}$$

with the average ratio $\left(\frac{l_b}{d_-}\right)_{avg}$ defined as in the case of the positive mutual inductance:

$$\left(\frac{l_b}{d_-}\right)_{avg} = \frac{b-(N-1)(w+g)}{a{-}w-\delta_-(w+g)} \tag{33}$$

and the term δ_- of the harmonic mean given as follows using the lower approximation expression from the harmonics series:

$$\begin{aligned}\delta_- &= \frac{\sum_{k=1}^{N-1}(N-k)}{\sum_{k=1}^{N-1}\frac{N-k}{k}} \\ &\approx \frac{1}{2}\frac{N(N-1)}{N\left[\ln(N-1)+0.57721+\frac{1}{2(N-1)}-\frac{1}{12(N-1)^2}\right]-N+1}.\end{aligned} \tag{34}$$

For the terms related to the width's negative mutual inductance M_-^w, the same development can be done, replacing $Q^l_{-_{avg}}$ by $Q^w_{-_{avg}}$ (a function of $\left(\frac{l_a}{d_-}\right)_{avg}$ obtained by exchanging b and a in (33)).

REFERENCES

[1] (2019). *Gartner Says 5.8 Billion Enterprise and Automotive IoT Endpoints Will be in Use in 2020*. [Online]. Available: https://www.gartner.com/en/newsroom/press-releases/2019-08-29-gartner-says-5-8-billion-enterprise-and-automotive-io

[2] *The Electronic Passport in 2019 and Beyond | Gemalto*. Accessed: Dec. 13, 2019. [Online]. Available: https://www.gemalto.com/govt/travel/electronic-passport-trends

[3] *Cards and Security Devices for Personal Identification, Contactless Proximity Objects, Part 2: RF Power and Signal Interface*, Standard ISO/IEC JTC 1/SC 17, 2016. [Online]. Available: https://www.iso.org/standard/73597.html

[4] C. E. Shannon, "A mathematical theory of communication," *Bell Syst. Tech. J.*, vol. 27, no. 3, pp. 379–423, 1948, doi: 10.1002/j.1538-7305.1948.tb01338.x.

[5] Wireless Power Consortium. (2017). *The Qi Wireless Power Transfer System Power Class 0 Specification*. [Online]. Available: https://www.wirelesspowerconsortium.com/knowledge-base/specifications/download-the-qi-specifications.html

[6] NFC Forum. (2019). *NFC Wireless Charging Specifications*. [Online]. Available: https://nfc-forum.org/our-work/specification-releases/specifications/nfc-forum-technical-specifications/

[7] *NFC Forum Specification Allows Wireless Charging of IoT Devices Using Shared Antenna—NFC Forum*. [Online]. Available: https://nfc-forum.org/nfc-forum-specification-allows-wireless-charging-of-iot-devices/-using-shared-antenna/

[8] Z. Xue, S. Fan, D. Li, L. Zhang, W. Gou, and L. Geng, "A 13.56 MHz, 94.1% peak efficiency CMOS active rectifier with adaptive delay time control for wireless power transmission systems," *IEEE J. Solid-State Circuits*, vol. 54, no. 6, pp. 1744–1754, Jun. 2019, doi: 10.1109/JSSC.2019.2894359.

[9] K. Noh, J. Amanor-Boadu, M. Zhang, and E. Sánchez-Sinencio, "A 13.56-MHz CMOS active rectifier with a voltage mode switched-offset comparator for implantable medical devices," *IEEE Trans. Very Large Scale Integr. (VLSI) Syst.*, vol. 26, no. 10, pp. 2050–2060, Oct. 2018, doi: 10.1109/TVLSI.2018.2845369.

[10] S. N. Daskalakis, G. Goussetis, and A. Georgiadis, "NFC hybrid harvester for battery-free agricultural sensor nodes," in *Proc. IEEE Int. Conf. RFID Technol. Appl. (RFID-TA)*, Sep. 2019, pp. 22–25, doi: 10.1109/RFID-TA.2019.8892237.

[11] U. Guler, Y. Jia, and M. Ghovanloo, "A reconfigurable passive RF-to-DC converter for wireless IoT applications," *IEEE Trans. Circuits Syst. II, Exp. Briefs*, vol. 66, no. 11, pp. 1800–1804, Nov. 2019, doi: 10.1109/TCSII.2019.2894562.

[12] D. Ye, Y. Wang, Y. Xiang, L. Lyu, H. Min, and C. R. Shi, "A wireless power and data transfer receiver achieving 75.4% effective power conversion efficiency and supporting 0.1% modulation depth for ASK demodulation," *IEEE J. Solid-State Circuits*, vol. 55, no. 5, pp. 1386–1400, May 2020, doi: 10.1109/JSSC.2019.2943871.

[13] C. Huang, T. Kawajiri, and H. Ishikuro, "A 13.56-MHz wireless power transfer system with enhanced load-transient response and efficiency by fully integrated wireless constant-idle-time control for biomedical implants," *IEEE J. Solid-State Circuits*, vol. 53, no. 2, pp. 538–551, Feb. 2018, doi: 10.1109/JSSC.2017.2767181.

[14] U. Guler, Y. Jia, and M. Ghovanloo, "A reconfigurable passive voltage multiplier for wireless mobile IoT applications," *IEEE Trans. Circuits Syst. II, Exp. Briefs*, vol. 67, no. 4, pp. 615–619, Apr. 2020, doi: 10.1109/TCSII.2019.2923534.

[15] Y. Jiang, K. Pan, T. Leng, and Z. Hu, "Smart textile integrated wireless powered near field communication (NFC) body temperature and sweat sensing system," *IEEE J. Electromagn., RF Microw. Med. Biol.*, early access, Jul. 22, 2019, doi: 10.1109/JERM.2019.2929676.

[16] A. Romputtal and C. Phongcharoenpanich, "IoT-linked integrated NFC and dual band UHF/2.45 GHz RFID reader antenna scheme," *IEEE Access*, vol. 7, pp. 177832–177843, 2019, doi: 10.1109/ACCESS.2019.2958257.

[17] Z. Zhang, H. Pang, A. Georgiadis, and C. Cecati, "Wireless power transfer—An overview," *IEEE Trans. Ind. Electron.*, vol. 66, no. 2, pp. 1044–1058, Feb. 2019, doi: 10.1109/TIE.2018.2835378.
[18] *MIFARE (Card) Coil Design Guide*, NXP and Mifare, Eindhoven, The Netherlands, 2006.
[19] Y. Lee, *Antenna Circuit Design*, document AN710, Mar. 2004. [Online]. Available: https://www.microchip.com/wwwAppNotes/AppNotes.aspx?appnote=en011776
[20] *How to Design a 13.56 MHz Customized Antenna*, document AN2866, STMicroelectronics, Feb. 2019. [Online]. Available: https://www.st.com/content/ccc/resource/technical/document/applicationnote/d9/29/ad/cc/04/7c/4c/1e/CD00221490.pdf/files/CD00221490.pdf/jcr:content/translations/en.CD00221490.pdf
[21] *Antenna Design Guide*, document AN 11740, NXP, Jun. 2018. [Online]. Available: https://www.nxp.com/docs/en/application-note/AN11740.pdf
[22] B. Couraud, T. Deleruyelle, E. Kussener, and R. Vauché, "Real-time impedance characterization method for RFID-type backscatter communication devices," *IEEE Trans. Instrum. Meas.*, vol. 67, no. 2, pp. 288–295, Feb. 2018, doi: 10.1109/TIM.2017.2769224.
[23] S. S. Mohan, M. del Mar Hershenson, S. P. Boyd, and T. H. Lee, "Simple accurate expressions for planar spiral inductances," *IEEE J. Solid-State Circuits*, vol. 34, no. 10, pp. 1419–1424, Oct. 1999, doi: 10.1109/4.792620.
[24] Carnets TSF. *Inductance Empirical Formula*. Accessed: Aug. 2019. [Online]. Available: https://www.carnets-tsf.fr/inductance.html
[25] H. Nagaoka, "The inductance coefficients of solenoids," *J. College Sci., Imperial Univ., Tokyo, Jpn.*, vol. 27, no. 3, pp. 1–33, 1909. [Online]. Available: https://www.carnets-tsf.fr/docs/Nagaoka1909.pdf
[26] F. Grover, *Tables for the Calculation of the Inductance of Circular Coils of Rectangular Cross Section* (Scientific Papers of the Bureau of Standards), vol. 18, no. 455. Washington, DC, USA: National Bureau of Standards, 1921, pp. 451–487. [Online]. Available: https://archive.org/details/tablesforcalcula18451grov/page/n4
[27] H. A. Wheeler, "Simple inductance formulas for radio coils," *Proc. Inst. Radio Eng.*, vol. 16, no. 10, pp. 1398–1400, Oct. 1928, doi: 10.1109/JRPROC.1928.221309.
[28] M. Gebhart and R. Szoncso, "Optimizing design of smaller antennas for proximity transponders," in *Proc. 2nd Int. Workshop Near Field Commun.*, Apr. 2010, pp. 77–82, doi: 10.1109/NFC.2010.12.
[29] D. Paret, *RFID and Contactless Smart Card Applications*. Hoboken, NJ, USA: Wiley, 2005.
[30] H. Greenhouse, "Design of planar rectangular microelectronic inductors," *IEEE Trans. Parts, Hybrids, Packag.*, vol. TPHP-10, no. 2, pp. 101–109, Jun. 1974, doi: 10.1109/TPHP.1974.1134841.
[31] ST. (2019). *NFC Antenna Design*. [Online]. Available: https://my.st.com/analogsimulator/html_app/antenna/#/
[32] S. Li and C. C. Mi, "Wireless power transfer for electric vehicle applications," *IEEE J. Emerg. Sel. Topics Power Electron.*, vol. 3, no. 1, pp. 4–17, Mar. 2015, doi: 10.1109/JESTPE.2014.2319453.
[33] K. Finkenzeller, *RFID Handbook: Fundamentals and Applications in Contactless Smart Cards, Radio Frequency Identification and Near-Field Communication*. Hoboken, NJ, USA: Wiley, Jun. 2010.
[34] T. Roz and V. Fuentes. (1999). *Using Low Power Transponders and Tags for RFID Applications*. [Online]. Available: https://www.mmsonline.com.cn/resupload/1270178170611_1.pdf
[35] Z. Shen, H. Wang, Y. Shen, Z. Qin, and F. Blaabjerg, "An improved stray capacitance model for inductors," *IEEE Trans. Power Electron.*, vol. 34, no. 11, pp. 11153–11170, Nov. 2019.
[36] D. Flynn, R. S. Dhariwal, and M. P. Y. Desmulliez, "A design study of microscale magnetic components for operation in the MHz frequency range," *J. Micromech. Microeng.*, vol. 16, no. 9, pp. 1811–1818, Jul. 2006, doi: 10.1088/0960-1317/16/9/008.
[37] D. Flynn and M. P. Y. Desmulliez, "Design, fabrication, and characterization of flip-chip bonded microinductors," *IEEE Trans. Magn.*, vol. 45, no. 8, pp. 3055–3063, Aug. 2009.
[38] D. Flynn and M. P. Y. Desmulliez, "Design methodology and fabrication process of a microinductor for the next generation of DC–DC power converters," *Microsyst. Technol.*, vol. 15, no. 8, pp. 1233–1243, 2009, doi: 10.1007/s00542-009-0820-7.
[39] D. Flynn, H. Lu, C. Bailey, and M. P. Y. Desmulliez, "Design, modeling and characterization of a microinductor for future DC-DC power converters," in *Proc. 2nd Electron. Syst.-Integr. Technol. Conf.*, Sep. 2008, pp. 577–582.
[40] A. Massarini, "Analytical approach to the calculation of parasitic capacitance between winding turns," in *Proc. IEEE 4th Int. Forum Res. Technol. Soc. Ind. (RTSI)*, Sep. 2018, pp. 1–4.
[41] Q. Yu and T. W. Holmes, "A study on stray capacitance modeling of inductors by using the finite element method," *IEEE Trans. Electromagn. Compat.*, vol. 43, no. 1, pp. 88–93, Feb. 2001.
[42] G. Grandi, M. K. Kazimierczuk, A. Massarini, and U. Reggiani, "Stray capacitances of single-layer solenoid air-core inductors," *IEEE Trans. Ind. Appl.*, vol. 35, no. 5, pp. 1162–1168, Sep./Oct. 1999.
[43] I. Schmidt and A. Enders, "Characterization and concept for optimization of planar spiral high power high frequency coils," in *Proc. IEEE Int. Symp. Electromagn. Compat.*, Aug. 2009, pp. 24–28.
[44] E. M. M. Costa, "Parasitic capacitances on planar coil," *J. Electromagn. Waves Appl.*, vol. 23, nos. 17–18, pp. 2339–2350, 2009, doi: 10.1163/156939309790416198.
[45] W. Li, "Wireless considerations in ocular implants based on microsystems," in *Handbook of Mems for Wireless and Mobile Applications* (Woodhead Publishing Series in Electronic and Optical Materials), D. Uttamchandani, Ed. Sawston, U.K.: Woodhead Publishing, 2013, pp. 424–462. [Online]. Available: http://www.sciencedirect.com/science/article/pii/B978085709271750013X
[46] D. Flynn, A. Toon, and M. P. Y. Desmulliez, "Manufacture and characterisation of micro-engineered DC-DC power converter using UV-LIGA process," *Electron. Lett.*, vol. 41, no. 24, pp. 1351–1353, Nov. 2005.
[47] D. Flynn, A. Toon, and M. Desmulliez, "Microscale magnetic components for the application of DC-DC converters operating in the 1-10 MHz range," in *Proc. Int. Symp. Electron. Mater. Packag.*, Dec. 2005, pp. 192–198.
[48] D. Flynn and M. Desmulliez, "A comparison of various magnetic thin films for the application of microscale magnetic components," *J. Phys., Conf. Ser.*, vol. 34, pp. 112–117, Apr. 2006, doi: 10.1088/1742-6596/34/1/019.
[49] H. Lu, D. Flynn, C. Bailey, and M. Desmulliez, "Computer modeling of a micro-manufactured one-turn inductor," in *Proc. Conf. High Density Microsyst. Design Packag. Compon. Failure Anal.*, Jun. 2006, pp. 37–42.
[50] H. Lu, D. Flynn, C. Bailey, and M. Desmulliez, "An analysis of a microfabricated solenoid inductor," in *Proc. 1st Electron. Systemintegr. Technol. Conf.*, vol. 1, Sep. 2006, pp. 556–561.
[51] J. A. Ferreira, "Improved analytical modeling of conductive losses in magnetic components," *IEEE Trans. Power Electron.*, vol. 9, no. 1, pp. 127–131, Jan. 1994.
[52] Z. Michalewicz and M. Schoenauer, "Evolutionary algorithms for constrained parameter optimization problems," *Evol. Comput.*, vol. 4, no. 1, pp. 1–32, 1996.
[53] *Identification Cards, Test Methods, Part 6: Proximity Cards*, Standard ISO/IEC 10373 6:2016, Jul. 2016. [Online]. Available: https://www.iso.org/standard/66290.html

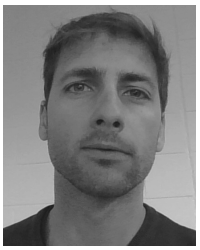

BENOIT COURAUD (Member, IEEE) received the Engineering degree from École Centrale de Lyon, Écully, France, in 2009, and the master's degree in electronic and electrical engineering from Shanghai Jiao Tong University, China, in 2009. His Ph.D. research focused on radio frequency identification power transfer optimization at ISEN, Toulon, France, and the IM2NP Laboratory, University of Aix-Marseille, Marseille, France. He is currently a Research Associate with Heriot-Watt University, working on artificial intelligence, market and optimization tools for renewable energies, and smart grids.

THIBAUT DELERUYELLE received the Engineering degree in electronics from the Polytechnical Engineering School, Polytech Lille, Lille, France, in 2006, and the Ph.D. degree in micro and nano electronics from the University of Aix-Marseille, Marseille, France, in 2010. In 2010, he joined the Superior Institute of Electronic and Digital (ISEN), Toulon, France, as a Research Lecturer. Since 2010, he has been an Associate Researcher with the RFID Sensor Team, IM2NP, Marseille, where he is also involved in integrated antennas, miniature antennas and radio frequency identification, Bluetooth, and the Internet-of-Things systems.

REMY VAUCHE received the M.Eng. degree in microelectronics and telecommunication from Polytech Marseille, Marseille, France, in 2008, the M.S. degree in microelectronics and nanoelectronics from Aix-Marseille University, Marseille, in 2008, and the Ph.D. degree in microelectronics from the University of Provence Aix-Marseille I, Marseille, in 2011. From 2011 to 2014, he was a Lecturer and a Researcher with the ISEN French Engineering School, Toulon, France. Since 2014, he has been an Associate Professor with Aix-Marseille University. He is a Member of the Integrated Circuits Design Team, Provence Nanosciences Microelectronics and Materials Laboratory, Marseille. His current research interests include the design of integrated circuits and systems for ultrawideband impulse radio, human body communications, and home-care applications.

DAVID FLYNN (Member, IEEE) received the B.Eng. degree (Hons.) in electrical and electronic engineering, the M.Sc. degree (Hons.) in microsystems, and the Ph.D. degree in microscale magnetic components from Heriot-Watt University, Edinburgh, U.K. He is currently a Professor of smart systems with Heriot-Watt University, where he is the Director and the Founder of the Smart Systems Group (SSG). He has over 135 publications and several international patents. His current research interests include energy systems, prognostics, reliability engineering, robotics, and microsystems. He is an Institute of Engineering and Technology (IET) Scholar as a recipient of the IET Leslie H Paddle Prize.

SPYRIDON NEKTARIOS DASKALAKIS (Member, IEEE) was born in Heraklion, Greece, in 1991. He received the Engineering Diploma and M.Sc. degrees in electrical and computer engineering from the Technical University of Crete (TUC), Chania, Greece, in 2014 and 2016, respectively. He is currently pursuing the Ph.D. degree with the School of Engineering and Physical Sciences, Heriot-Watt university, Edinburgh, U.K. His current research interests include low-power, low-cost wireless sensor networks, and energy harvesting. He was a recipient of the Fellowship Award by the Clinton Global Initiative University 2014, USA; the Onassis Foundation (Graduate Studies 2015/16 Scholarship); the Lloyds Register Foundation (LRF); and the International Consortium in Nanotechnology (ICON). He was also a recipient for two short-term scientific mission grants from COST Action IC1301 WiPE of the School of Electrical and Computer Engineering, Georgia Institute of Technology, Atlanta, GA, USA, in 2016, and the Centre Tecnologic de Telecomunicacions de Catalunya, Barcelona, Spain, in 2015, the IEEE MTT-S Graduate Fellowship for 2019, and the first and second Year Postgraduate Research Prizes from Heriot-Watt University.